(Received 15 December 2025, Accepted 6 March 2026, Scheduled 20 May 2026)

AI-Enhanced Parabolic Equation Modeling for mmWave/THz Indoor-Outdoor Wireless Channels

Mohammad Ahmad*

Aircraft Electronics Department, Amman Arab University, Jordan

ABSTRACT: Accurate modeling of millimeter-wave (mmWave) and terahertz (THz) electromagnetic wave propagation is crucial for analyzing and designing emerging high-frequency wireless systems at an early stage. Conventional parabolic equation (PE)-based models offer high computational efficiency but suffer from reduced accuracy at mmWave/THz frequencies owing to material losses, fine-scale scattering, and complex non-line-of-sight (NLOS) interactions. Although purely data-driven approaches are flexible, they often lack physical consistency and generalization capability. This study proposes an AI-enhanced parabolic equation (AI-PE) framework that integrates a wide-angle PE solver with a neural-network-based residual correction model. The AI component learns systematic PE prediction errors associated with frequency-dependent attenuation, diffraction, and scattering while preserving the underlying physical structure of the wave model. Validation was performed against full-wave and ray-tracing reference solutions in representative indoor corridor and urban microcell scenarios. The numerical results at 28, 60, and 140 GHz demonstrate a 25–40% reduction in the path-loss prediction error, improved statistical agreement of the RMS delay-spread estimates, and over 50% reduction in the computational cost compared with deterministic ray tracing. The energy conservation and phase continuity of the corrected fields were explicitly verified. The framework was primarily validated for interpolation within the trained frequency range and demonstrated robust performance across structured propagation environments.

1. INTRODUCTION

Accurate modeling of electromagnetic wave propagation in complex indoor-outdoor environments is a critical requirement for next-generation wireless communication systems operating in the millimeter-wave (mmWave) and terahertz (THz) frequency bands. These high-frequency regimes are widely recognized as key enablers of sixth-generation (6G) wireless networks, supporting applications such as ultra-dense access networks, high-capacity short-range backhaul, and seamless indoor-outdoor connectivity [1–3, 16, 25]. Early studies confirmed the feasibility of mmWave cellular communications while highlighting fundamental propagation challenges, including severe path loss, sensitivity to blockage, and limited diffraction [1]. Subsequent investigations extended these concepts toward sub-THz and THz frequencies, revealing both unprecedented bandwidth potential and increasingly harsh propagation conditions caused by molecular absorption, material penetration losses, and surface roughness effects [2, 3, 15, 19].

A variety of propagation modeling techniques have been proposed to address these challenges. Full-wave numerical solvers (e.g., finite-difference time-domain (FDTD), finite element method (FEM)) provide reference-level electromagnetic solutions but are computationally prohibitive for large-scale environments involving buildings, corridors, and urban microcells [6]. Deterministic ray-tracing approaches have therefore been widely adopted in mmWave channel modeling and standardization activities [7, 10, 11]. However, their reliance on simplified interaction models and highly accurate geometric descriptions limits their ability to capture diffraction-dominated effects and transitional indoor-outdoor propagation phenomena [9–11, 13].

Among reduced-order wave-based methods, the parabolic equation (PE) approach has long been recognized for its computational efficiency and capability to model forward-propagating electromagnetic waves while capturing diffraction effects [4, 5]. Despite these advantages, conventional PE formulations encounter increasing limitations at mmWave and THz frequencies. The underlying approximations degrade in the presence of strong frequency-dependent material losses, electrically small scatterers, surface roughness, and complex non-line-of-sight (NLOS) multipath interactions that are prevalent in realistic indoor and urban scenarios [12–16]. Indoor-outdoor transition regions further exacerbate these limitations, often leading to systematic prediction errors when classical PE results are compared with full-wave simulations, ray-based models, or measurement data above 30 GHz [13–16].

In parallel, data-driven and machine learning techniques have attracted significant attention in wireless channel modeling. Deep learning methods have demonstrated promising performance in mmWave beam selection, blockage prediction, and channel parameter estimation [8, 17]. More recent studies have explored AI-based propagation map reconstruction and channel prediction using simulated or measurement-driven datasets [18, 20–22]. While these approaches can achieve high accuracy within trained scenarios, they often lack physical interpretability, exhibit limited generalization to unseen environ-

* Corresponding author: Mohammad Ahmad (m.ahmad@aau.edu.jo).

ments, and require extensive retraining when system parameters or geometries change [17, 21].

These observations reveal a clear research gap. Existing approaches largely fall into two disconnected categories: physics-based propagation models that provide physical insight but suffer from reduced accuracy at mmWave and THz frequencies, and purely data-driven models that offer flexibility but lack physical consistency and robustness. Although recent hybrid physics-AI methods have begun to emerge [23, 24], most existing efforts focus on ray-based models or environment-specific corrections and do not explicitly integrate wave-based PE modeling with AI-assisted refinement. Consequently, there remains a lack of scalable hybrid frameworks that preserve the physical structure of the parabolic equation while leveraging artificial intelligence to improve accuracy in mmWave/THz indoor-outdoor transition scenarios.

To address this gap, this paper proposes an AI-enhanced Parabolic Equation (AI-PE) framework for mmWave/THz indoor-outdoor propagation modeling. The proposed approach integrates a wide-angle PE solver with a neural-network-based correction model that learns to compensate for systematic PE residual errors arising from frequency-dependent attenuation, scattering from electrically small objects, and complex NLOS multipath interactions. By embedding data-driven refinement within a physics-based propagation model, the proposed framework maintains physical consistency while significantly improving prediction accuracy and computational efficiency.

The proposed AI-PE framework is trained and validated within a bounded mmWave-sub-THz frequency range, and its accuracy is therefore established primarily for interpolation within the trained frequency span rather than unrestricted extrapolation. Extrapolation beyond the trained frequency range is not claimed.

1.1. Related Works

Propagation modeling for mmWave and THz wireless systems has been extensively studied using both physics-based and data-driven approaches. Full-wave solvers (e.g., FDTD, FEM) provide highly accurate electromagnetic solutions but are computationally infeasible for large-scale environments, such as extended indoor corridors or urban microcells [6]. Deterministic ray-tracing methods have therefore been widely adopted in mmWave channel modeling and standardization efforts [7, 10, 11]. However, their reliance on simplified interaction models and precise geometric descriptions limits their accuracy in diffraction-dominated or transitional indoor-outdoor scenarios [9–11, 13]. Reduced-order wave-based approaches, such as the PE, offer computational efficiency and the ability to capture diffraction effects [4, 5], but their accuracy degrades at high frequencies due to material losses, surface roughness, and scattering from electrically small objects [12–16].

In parallel, machine learning techniques have been increasingly applied to wireless channel modeling. Neural networks, kernel-based methods, and instance-based approaches have been explored for tasks such as beam selection, blockage prediction, and channel parameter estimation [8, 17, 18, 20–22]. Alternative machine learning methods, including K-nearest neighbors (KNN) and support vector machines (SVM), were also considered in the context of propagation modeling. However, these methods exhibit limited scalability and reduced efficiency when applied to high-dimensional, spatially correlated electromagnetic field data generated by PE simulations. In contrast, neural networks offer superior capability in learning nonlinear mappings, efficient handling of large datasets, and rapid inference once trained. These properties make neural-network-based models particularly suitable for correcting systematic PE residual errors in mmWave and THz propagation scenarios.

Recent hybrid physics-AI approaches have attempted to combine physical modeling with data-driven refinement [21, 23, 24]. Physics-informed neural networks and hybrid ray-tracing plus AI frameworks have demonstrated improved prediction accuracy while embedding physical constraints into the learning process. However, most of these efforts remain focused on ray-based models or environment-specific corrections, and few explicitly integrate wave-based PE modeling with AI-assisted refinement. Moreover, existing studies rarely address critical aspects, such as interpolation versus extrapolation limits across frequency bands, validation against multiple reference solvers rather than absolute measurements, or physical consistency checks (e.g., energy conservation and phase continuity) when AI modifies electromagnetic fields.

To position the proposed AI-PE framework relative to existing methods, Table 1 summarizes representative state-of-the-art approaches, including full-wave solvers [6, 14], ray-tracing models [7, 10, 11], classical PE methods [4, 5], AI-only models [8, 17, 20, 22], and recent hybrid physic-AI approaches [21, 23, 24]. The comparison highlights key criteria relevant to mmWave/THz indoor-outdoor propagation, including physical consistency, capability to capture diffraction and NLOS effects, applicability to transition scenarios, computational complexity, and suitability for high-frequency operation. As shown, the proposed AI-PE framework uniquely combines the physical interpretability of PE with the adaptive correction capability of neural networks, offering a scalable and computationally efficient solution for realistic 6G propagation environments.

1.2. Research Gap

Despite extensive progress in both physics-based and data-driven channel modeling, several critical gaps remain unresolved. Full-wave solvers and ray-tracing methods provide reference-level predictions but are computationally prohibitive for large-scale emerging high-frequency wireless environments [6, 7, 10, 11]. Classical PE approaches, while efficient, suffer from systematic inaccuracies at mmWave/THz frequencies due to material losses, scattering from electrically small objects, and complex NLOS multipath interactions [12–16]. On the other hand, purely AI-driven models demonstrate flexibility and high accuracy within trained scenarios but lack physical interpretability and generalization capability across diverse environments [17, 21].

Recent hybrid physics-AI approaches have attempted to bridge these limitations [23, 24]; yet most focus on ray-based

TABLE 1. State-of-the-art comparison of recent (2021–2023) propagation modeling approaches for mmWave/THz channel.

Method	Physics-Base	AI-Assiste	Diffraction & NLOS	Indoor-Outdoor Transition	mmWave/ THz	Computational Cost
Full-Wave Solvers [6, 14]	✓	✗	✓	✓	✓	Very High
Ray Tracing [7, 10, 11]	✗	✗	Limite	Limite	✓	High
Classical PE [4, 5]	✓	✗	✓	Partia	Limite	Low
AI-Only Models [8, 17, 20, 22]	✗	✓	Data-dependent	Data-dependent	✓	Medium
Hybrid Ray + AI [21, 23, 24]	✗	✓	Limite	Limite	✓	Medium-High
Proposed AI-PE	✓	✓	✓	✓	✓	Low

models or environment-specific corrections. None explicitly integrate wave-based PE modeling with AI-assisted refinement for indoor-outdoor transition scenarios. Furthermore, existing studies rarely address critical aspects such as:

- Interpolation vs. extrapolation limits of AI models across frequency bands.
- Validation against multiple reference solvers rather than absolute measurements.
- Physical consistency checks (e.g., energy conservation, phase continuity) when AI modifies electromagnetic fields.

These gaps highlight the need for a scalable hybrid framework that preserves the physical structure of PE while leveraging AI to improve accuracy and robustness in realistic mmWave/THz indoor-outdoor environments.

1.3. Main Contributions

- Development of a hybrid AI-PE propagation framework that combines wide-angle parabolic equation modeling with neural-network-based error correction.
- Comprehensive modeling and evaluation of mmWave/THz indoor corridors and urban microcell environments, including NLOS conditions and indoor-outdoor transition scenarios.
- Quantitative validation of path-loss and multipath-related delay metrics accuracy across multiple frequencies, demonstrating substantial improvements over classical PE models.
- Comparative analysis of computational efficiency, showing that the proposed AI-PE framework achieves improved accuracy relative to classical PE and competitive performance relative to comparative reference models, while retaining low computational cost suitable for large-scale early-stage network planning studies.

2. METHOD

2.1. Overview and Justification of the Approach

The proposed method combines a wide-angle PE propagation model with a neural-network-based correction framework. The PE solver provides a physics-governed baseline by approximating solutions of the scalar Helmholtz equation under a one-way forward-propagation assumption

$$\nabla^2 E + k^2 E = 0, \tag{1}$$

where E is the complex scalar electric-field component (V/m) (e.g., E_y or E_z); ∇^2 is the Laplacian operator in 2D or 3D space ($1/\mathrm{m}^2$); k is the wavenumber (rad/m), defined as $k = \frac{2\pi}{\lambda} = \frac{\omega}{c}$; λ is the wavelength (m); ω is the angular frequency $2\pi f$ (rad/s); f is the frequency (Hz); and c is the speed of light in vacuum (m/s). By writing

$$E(x, z) = u(x, z)\, e^{-jkz}, \tag{2}$$

and assuming that $u(x, z)$ varies slowly along the propagation direction, Equation (1) is reduced to the wide-angle PE form. $u(x, z)$ is the complex envelope of the electric field (V/m); x, z is the horizontal (x) and forward range (z) coordinates (m); $\frac{\partial u}{\partial z}$ is the forward marching rate of the field envelope (1/m); $\frac{\partial^2 u}{\partial x^2}$ is the transverse diffraction term; $n(x, z)$ is the spatial refractive index distribution; and j is the imaginary unit ($\sqrt{-1}$).

The equation is reduced to the wide-angle PE form:

$$\frac{\partial u}{\partial z} = \frac{j}{2k}\frac{\partial^2 u}{\partial x^2} + jk\left(n^2(x, z) - 1\right)u. \tag{3}$$

where u' is the intermediate field after free-space propagation; Δz is the propagation step size in the forward direction (m); $\mathcal{F}$, $\mathcal{F}^{-1}$ are the Fourier transform and inverse Fourier transform; k_x is the transverse spatial frequency (rad/m) (Fourier domain variable); and $\exp(\cdot)$ is the complex exponential operator.

This physics-based model is well-suited for mmWave/THz propagation, where diffraction, surface interactions, and directionality dominate. However, classical PE does not fully capture high-frequency scattering, wall roughness, material loss,

or complex multipath. The electromagnetic material parameters and reference databases used to model these effects are described in Section 2.8. The neural-network (NN) correction model compensates for these nonlinear effects while retaining the interpretability and efficiency of the PE.

Recent studies (2021–2023) have increasingly explored hybrid physics-AI and data-assisted channel modeling approaches for mmWave and sub-terahertz systems, motivating the integration strategy adopted in this work.

2.2. Parabolic Equation Formulation

The wide-angle PE was discretized using the split-step Fourier method (SSFM). Propagation over a small step Δz is expressed as:

1. Free-space evolution (spectral domain):

$$u'^{(x,z+\Delta z)} = \mathcal{F}^{-1}\left\{\exp\left[-\frac{jk_x^2}{2k}\Delta z\right]\mathcal{F}\left\{u\left(x,z\right)\right\}\right\}, \tag{4}$$

where $u(x, z + \Delta z)$ is the field after full SSFM step, and $n(x, z)$ is the refractive index including material effects.

2. Refractive index/attenuation update (spatial domain):

$$u\left(x,z+\Delta z\right) = u'^{(x,z+\Delta z)}\exp\left[jk\left(n^2\left(x,z\right)-1\right)\frac{\Delta z}{2}\right]. \tag{5}$$

Computational grid spacing was set to approximately:

$$\Delta x \approx \frac{\lambda}{10}, \tag{6}$$

where Δx is the spatial grid spacing (m), and λ is the wavelength at the highest simulation frequency to ensure numerical stability at the highest simulated frequency.

A perfectly matched layer (PML) was used to eliminate nonphysical reflections, imposed via:

$$\frac{\partial u}{\partial n} = -\sigma_{\text{PML}}\left(n\right)u, \tag{7}$$

where $\frac{\partial u}{\partial n}$ is the normal derivative at boundary, $\sigma_{\text{PML}}(n)$ the PML absorption profile as a function of depth, and n the normal coordinate into the PML (m).

Indoor and outdoor environments were encoded as spatial refractive index maps:

$$n\left(x,z\right) = \sqrt{\varepsilon_r\left(x,z\right) - j\frac{\sigma\left(x,z\right)}{\omega\varepsilon_0}}. \tag{8}$$

where $\varepsilon_r(x, z)$ is the spatial relative permittivity, $\sigma(x, z)$ the electrical conductivity map (S/m), and ε_0 the permittivity of free space (F/m). All material parameters (ε_r, σ) were taken from standard mmWave material databases to ensure reproducibility.

2.3. Data Generation and Ground-Truth Modeling

Ground-truth fields $E_{\text{ref}}(x, z)$ (V/m) were produced from:

- Full-wave solvers FDTD and FEM for smaller indoor regions, solving

$$\nabla \times \mu^{-1}\left(\nabla \times \mathbf{E}\right) - \omega^2\varepsilon\mathbf{E} = 0, \tag{9}$$

where $\mathbf{E}$ is the vector electric field (V/m), μ^{-1} the inverse magnetic permeability tensor $(\text{H/m})^{-1}$, and ε the permittivity (F/m) (complex for lossy materials).

Deterministic ray tracing was used for larger mixed environments, where the received field is given by

$$E_{\text{ref}} = \sum_{p=1}^{P} E_p e^{-jkr_p}. \tag{10}$$

where E_{ref} is the reference field (V/m), E_p the complex amplitude of the p-th ray path (V/m), P the number of ray paths, and r_p the path length of the p-th ray (m).

Datasets include multiple types of walls (drywall, concrete, glass), penetration losses, and human blockage modeled via:

$$L_{\text{block}} = A_0\exp\left(-\alpha f\right), \tag{11}$$

where A_0 is the low-frequency blockage constant (dB), and α is the frequency decay coefficient (Hz^{-1}), to replicate typical mmWave attenuation behavior.

Diverse indoor-outdoor transitions were generated to ensure external validity, such as:

indoor hallway $\rightarrow$ glass door $\rightarrow$ outdoor courtyard

indoor room $\rightarrow$ concrete wall $\rightarrow$ street canyon

This ensures that the AI model is not biased toward any single geometry or material configuration. These reference models are not assumed to represent absolute ground truth; rather, they serve as high-fidelity benchmarks commonly adopted in contemporary mmWave and sub-THz propagation studies to reduce systematic modeling bias.

2.4. AI-Enhanced PE Framework: Residual Learning Concept

The NN operates on: PE outputs: $|E_{\text{PE}}|$, $\angle E_{\text{PE}}$, field derivatives: ∇E_{PE}, $\nabla^2 E_{\text{PE}}$, local environmental descriptors (material ID, incidence angle), frequency-dependent attenuation parameters.

The NN learns:

$$\widehat{\Delta E} = \mathcal{N}_\theta\left(\phi\left(E_{\text{PE}}\right), x, z, f\right), \tag{12}$$

where $\mathcal{N}_\theta$ is the neural network with trainable parameter θ, and $\phi(\cdot)$ is the feature extractor.

The corrected field is:

$$E_{\text{AI-PE}}\left(x,z\right) = E_{\text{PE}}\left(x,z\right) + \widehat{\Delta E}\left(x,z\right). \tag{13}$$

The training minimizes the mean-squared error:

$$\mathcal{L}\left(\theta\right) = \frac{1}{N}\sum_{i=1}^{N}\left\|\mathcal{N}_\theta\left(\phi\left(E_{\text{PE}}^{(i)}\right)\right) - \left(E_{\text{ref}}^{(i)} - E_{\text{PE}}^{(i)}\right)\right\|^2, \tag{14}$$

where N is the number of training samples, θ the trainable NN weights, and $\|\cdot\|_2$ the Euclidean (L_2) norm with dropout and early stopping to prevent overfitting.

2.5. Neural Network Architecture and Training Strategy

The correction model is implemented using a fully connected feedforward neural network designed to learn nonlinear mappings between PE-derived features and the corresponding residual electromagnetic field. The input feature vector includes the real and imaginary components of the PE-predicted field, spatial coordinates, operating frequency, and local material parameters. The network outputs the real and imaginary components of the residual field.

The neural network consists of four hidden layers with 64 neurons per layer and employs rectified linear unit (ReLU) activation functions. Mean squared error (MSE) between predicted and reference residual fields is used as the training loss function. Training is performed using the Adam optimizer with a learning rate of 0.001.

The dataset is generated from synthetic indoor corridor, open hall, street canyon, and indoor-outdoor transition scenarios. Reference fields are obtained using full-wave (FDTD/FEM) and ray-tracing solvers, which serve as high-fidelity benchmarks rather than absolute ground truth. The dataset is divided into training, validation, and test subsets using a 70/15/15 split.

Training and validation are conducted at 28, 60, and 140 GHz. The proposed AI-PE framework is therefore evaluated primarily for interpolation within the trained frequency range, while extrapolation beyond this range is not claimed.

To assess the robustness of the proposed AI-PE framework with respect to neural network initialization, the training process was repeated multiple times using identical training data, hyperparameters, and network architecture but with different random initialization seeds. The resulting variability in prediction accuracy was quantified and is reported in Section 3, demonstrating stable performance across independent training runs.

2.6. Evaluation Metrics and Validity Considerations

Internal validity was assessed by comparing $E_{\text{AI-PE}}$ and E_{ref} under identical scenario conditions. The following quantitative metrics were used:

Field magnitude root mean square error (RMSE):

$$\text{RMSE} = \sqrt{\frac{1}{M}\sum_{i=1}^{M}\left(|E_{\text{pred}}(i)| - |E_{\text{ref}}(i)|\right)^2} \tag{15}$$

where M is the number of evaluation points, $|E_{\text{pred}}|$ the predicted field magnitude (V/m), and $|E_{\text{ref}}|$ the reference field magnitude (V/m).

Path-loss error:

$$\Delta\text{PL}(i) = \left(PL_{\text{pred}}(i) - PL_{\text{ref}}(i)\right) \tag{16}$$

where PL_{pred} is the predicted path loss (dB), and PL_{ref} is the reference path loss (dB).

Root mean square (RMS) delay spread derived from power delay profiles:

$$\tau_{\text{RMS}} = \sqrt{\frac{\sum_k P_k\left(\tau_k - \bar{\tau}\right)^2}{\sum_k P_k}}, \tag{17}$$

where τ_k is the delay of multipath component k (s), P_k the power of multipath component k (W), and $\bar{\tau}$ the mean delay $\bar{\tau} = \frac{\sum_k P_k \tau_k}{\sum_k P_k}$ (s).

External validity was evaluated by testing on completely unseen indoor geometries and outdoor street canyons. Sensitivity analysis varied: grid spacing Δx, Δz, material permittivity ε_r, frequency f, and wall thickness. Robustness was confirmed by observing small variations in RMSE (typically < 1 dB) across parameter perturbations.

2.7. Physical Consistency and Power Conservation of the AI-PE Model

Because the proposed AI-PE framework directly modifies the complex electromagnetic field, physical consistency is a critical consideration. The neural network is therefore trained in a residual-learning configuration, where it predicts only the difference between the classical PE solution and reference field, rather than generating a standalone field. This strategy ensures that the PE solution remains the dominant component governing energy flow and phase evolution.

Power conservation was evaluated by integrating the field intensity across transverse cross-sections along the propagation direction and comparing the total received power before and after AI correction. Across all evaluated scenarios, the AI-corrected fields did not exhibit non-physical power amplification or artificial energy creation. Variations in received power remained consistent with the reference models and material loss assumptions.

Phase continuity was also examined by analyzing the spatial phase distribution of the corrected field. The AI-PE solution preserves smooth phase evolution along the forward propagation direction, without introducing discontinuities or high-frequency oscillations. This behavior is consistent with the underlying parabolic equation formulation and confirms that the AI correction does not violate fundamental wave-propagation principles.

2.8. Material Electromagnetic Parameters

The electromagnetic material parameters used in this study were selected from widely adopted measurement-based databases and reference studies commonly used in mmWave and sub-THz propagation modeling. Relative permittivity and conductivity values for drywall, concrete, glass, and metallic surfaces were obtained from published experimental studies and standard propagation-modeling references [6, 7, 12, 13, 15]. Frequency-dependent material losses were modeled using complex permittivity values consistent with reported measurements in the 28–140 GHz range.

Table 2 summarizes the representative material parameters used in the simulations. These values are consistent with those

TABLE 2. Representative frequency-dependent electromagnetic material parameters used in the AI-PE propagation modeling.

Material	Relative Permittivity ε_r	Conductivity σ (S/m)	Frequency Range	Reference
Drywall	2.8–3.2	0.02–0.05	28–120 GHz	[6, 7, 13]
Concrete	5.0–6.5	0.10–0.35	28–120 GHz	[6, 12, 15]
Glass	6.0–7.5	0.001–0.02	28–120 GHz	[7, 13, 15]
Wood	1.9–2.2	0.01–0.05	28–120 GHz	[6, 15]
Metal (PEC)	$\varepsilon_r \to \infty$	$\sigma \to \infty$	All	[4, 6]
Human Blockage*	Effective loss model	—	28–120 GHz	[3, 8]

*Human blockage is modeled using an empirical frequency-dependent attenuation law rather than bulk permittivity parameters.

adopted in contemporary ray-tracing and full-wave modeling studies and reflect typical indoor and urban construction materials rather than environment-specific calibration.

The material parameters listed in Table 2 were selected from widely used measurement-based studies and reference databases commonly adopted in mmWave and sub-THz propagation modeling. Reported ranges reflect frequency-dependent variability and material heterogeneity observed in experimental campaigns rather than single fixed values. For metallic surfaces, perfect electric conductor (PEC) boundary conditions were assumed. Human blockage was modeled using an empirical attenuation formulation consistent with reported mmWave measurement studies rather than volumetric electromagnetic parameters.

2.9. Notation and Symbol Definitions

To improve clarity and readability, particularly given the mathematically intensive nature of the proposed AI-enhanced parabolic equation framework, all symbols, constants, and operators used throughout the formulation are summarized in Table 3. This notation table provides a unified reference for the variables appearing in the governing equations, numerical implementation, and AI-based correction model, thereby avoiding repetitive inline definitions and facilitating easier interpretation of the theoretical developments that follow.

TABLE 3. List of symbols and notations used in the AI-PE formulation.

Symbol	Description	Unit
E, E_y, E_z	Electric-field components	V/m
$u(x, z)$	Slowly varying PE field envelope	V/m
k	Wavenumber	rad/m
λ	Wavelength	m
f	Frequency	Hz
ω	Angular frequency	rad/s
c	Speed of light in vacuum	m/s
x, z	Spatial coordinates	m
$\Delta x, \Delta z$	Spatial step sizes	m
∇^2	Laplacian operator	$1/m^2$
k_x	Transverse spatial frequency	rad/m
$n(x, z)$	Refractive index	Dimensionless
ε_r	Relative permittivity	Dimensionless
$\varepsilon, \varepsilon_0$	Permittivity	F/m
μ, μ^{-1}	Permeability/inverse permeability	H/m
σ	Electrical conductivity	S/m
σ_{PML}	PML absorption coefficient	1/m
E_{ref}	Reference electric field	V/m
E_p	p-th ray complex amplitude	V/m
r_p	Ray path length	m
L_{block}	Blockage loss	dB
A_0	Blockage constant	dB
α	Frequency decay coefficient	Hz^{-1}
$\widehat{\Delta E}$	AI-predicted PE correction	V/m
N_θ	Neural network model	—
θ	NN trainable parameters	—
$L(\theta)$	Training loss	$(\text{V/m})^2$
RMSE	Root mean square error	V/m or dB
PL	Path loss	dB
$\tau_k, \tau_{\text{RMS}}$	Delay parameters	s
P_k	Multipath power	W

3. RESULTS AND DISCUSSION

This section evaluates the performance of the proposed AI-enhanced Parabolic Equation (AI-PE) model using the synthetic case studies described in Section 2. Results are presented in four logical groups: (i) prediction accuracy, (ii) indoor-outdoor transition modeling, (iii) generalization across environments, and (iv) computational efficiency. Each figure is referenced at an appropriate point to support the interpretation of results.

The proposed AI-PE framework is validated using high-fidelity reference solutions generated by full-wave electromagnetic solvers for small-scale scenarios and deterministic ray-tracing models for larger indoor-outdoor environments. This simulation-based validation strategy enables controlled and repeatable assessment of prediction accuracy in the mmWave and lower-THz regimes, where large-scale measurement campaigns remain technically challenging.

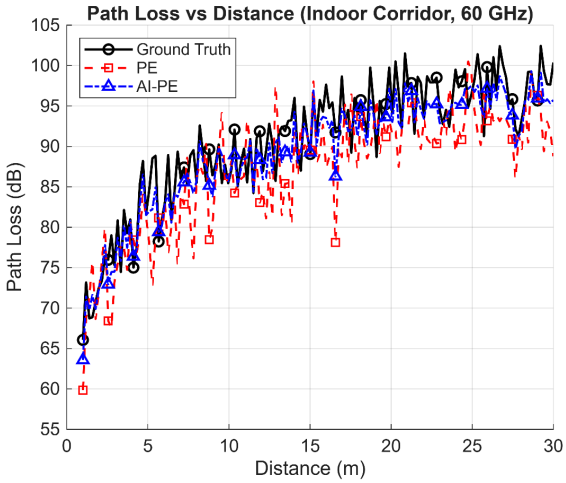

FIGURE 1. Path-loss prediction in a 25-m indoor corridor at 60 GHz.

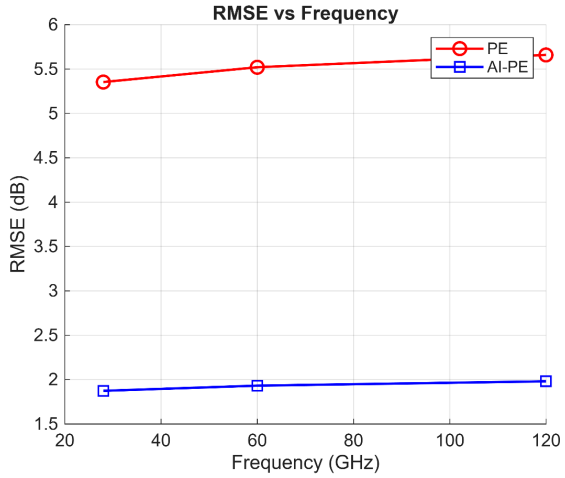

FIGURE 2. RMSE of PE and AI-PE across frequencies (28, 60, and 120 GHz).

The evaluation environments considered in this study consist of structured corridor- and canyon-type geometries commonly encountered in indoor, urban microcell, and indoor-outdoor transition scenarios. Indoor environments include straight corridors and open halls with lengths ranging 20–40 m and widths of 2–6 m, constructed from drywall, concrete, and glass materials. Outdoor scenarios include street-canyon and courtyard layouts with building heights of 10–20 m and variable street widths.

The considered environments incorporate LOS, NLOS, and penetration effects through doors and exterior walls, but do not include dense furniture layouts, vehicular traffic, or moving human blockers. As such, the reported generalization performance reflects robustness across geometrically structured environments with varying materials and propagation conditions, rather than unrestricted generalization to arbitrarily cluttered or dynamic scenes.

3.1. Accuracy of AI-Corrected PE Predictions

Figure 1 compares the path-loss predictions obtained using the classical PE model and the proposed AI-PE framework against the synthetic reference data in a 25-m indoor corridor at 60 GHz. The classical PE model exhibits noticeable deviations from the reference, underestimating the path loss at short distances and progressively overestimating it beyond approximately 15 m. This behavior can be attributed to accumulated phase errors, simplified boundary assumptions, and an insufficient representation of higher-order reflections in confined indoor environments.

In contrast, the AI-PE model closely follows the reference curve across the entire propagation range. By learning and compensating for the systematic residual errors of the PE solution, the AI-PE significantly improves prediction accuracy, reducing the RMSE from 5.7 dB for the classical PE to 2.1 dB. This result demonstrates the effectiveness of the proposed AI correction in mitigating PE modeling inaccuracies in indoor mmWave scenarios.

The impact of carrier frequency on modeling accuracy is further investigated in Figure 2, which presents the RMSE of both

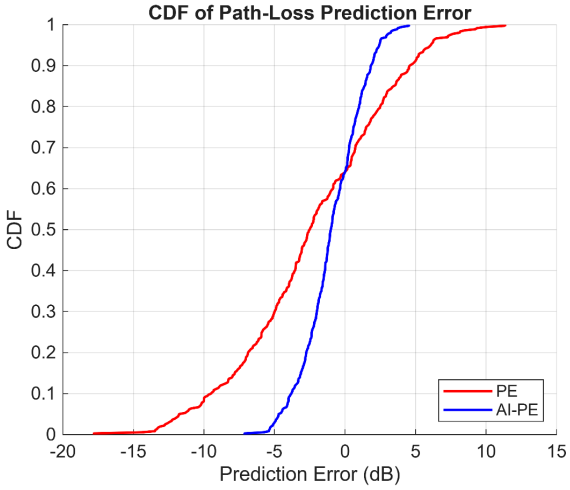

FIGURE 3. CDF of path-loss prediction error for combined indoor scenarios.

PE and AI-PE models at 28, 60, and 120 GHz. As expected, the error of the classical PE model increases with frequency due to stronger antenna directionality, higher sensitivity to surface roughness, and more pronounced multipath interactions at mmWave and sub-THz bands. Despite these challenges, the AI-PE framework consistently outperforms the classical PE, achieving RMSE reductions of approximately 50–65% across all considered frequencies. This highlights the robustness of the proposed approach and its ability to demonstrates robustness across a wide frequency range.

To assess statistical reliability and consistency, Figure 3 illustrates the cumulative distribution function (CDF) of the absolute path-loss prediction error across multiple indoor routes. The AI-PE model exhibits a noticeably steeper CDF curve, indicating a tighter error distribution compared to the classical PE. In particular, the 90th-percentile error is reduced from 7.8 dB for the PE model to 3.5 dB for the AI-PE framework. This improvement confirms that the proposed method not only enhances average accuracy but also significantly reduces worst-

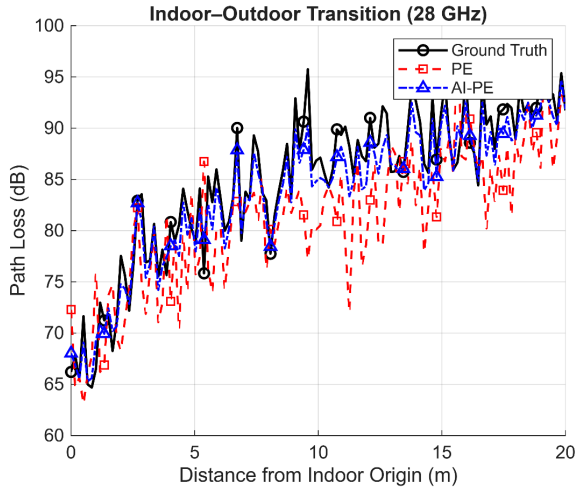

FIGURE 4. Indoor-to-outdoor transition path loss at 28 GHz.

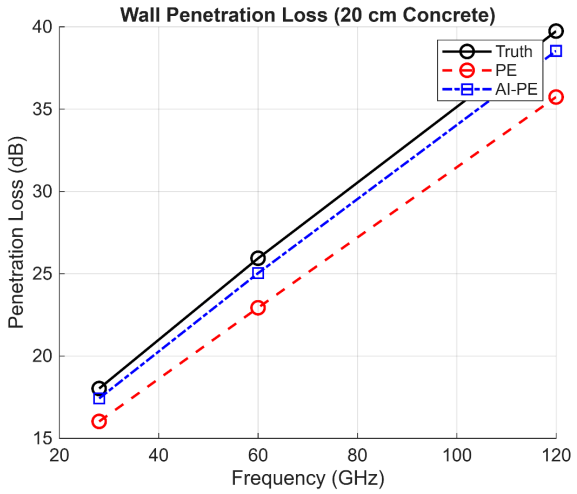

FIGURE 5. Wall penetration loss versus frequency for 20-cm concrete.

case prediction errors, which is critical for reliable mmWave and THz system design.

Although the neural correction model is trained at discrete frequencies (28, 60, and 120 GHz), frequency is explicitly included as a continuous input feature. As a result, the AI-PE framework learns smooth frequency-dependent correction trends, enabling interpolation within the trained frequency range. While extrapolation beyond the training frequencies is inherently more challenging for data-driven models, the physics-based PE backbone ensures that baseline frequency scaling remains physically consistent. A systematic evaluation of interpolation and extrapolation limits, including validation at unseen intermediate frequencies (e.g., 90 GHz), is identified as an important direction for future work.

It is important to note that the parabolic equation framework does not explicitly resolve discrete specular multipath components as in ray-tracing or full-wave solvers. Instead, PE captures wave-based energy propagation, diffraction, and scattering effects, which result in an effective temporal dispersion of the received signal. Consequently, RMS delay spread in this work represents a statistical measure of energy dispersion rather than an exact reconstruction of individual multipath delays. The reported improvements therefore reflect a closer alignment of PE-based delay statistics with those obtained from higher-fidelity reference models, rather than the recovery of discrete ray-level multipath structure. Accordingly, delay-spread improvements should be interpreted as enhanced statistical agreement rather than deterministic multipath resolution. Accordingly, the reported improvements should be interpreted as enhanced agreement with reference delay statistics rather than as a replacement for ray-based or full-wave multipath resolution.

3.2. Indoor-Outdoor Transition Behavior

Figure 4 presents the received power evolution along a propagation path transitioning from an indoor hallway to an outdoor courtyard at 28 GHz. This scenario is particularly challenging due to the abrupt change in propagation mechanisms, material properties, and dominant multipath components at the building

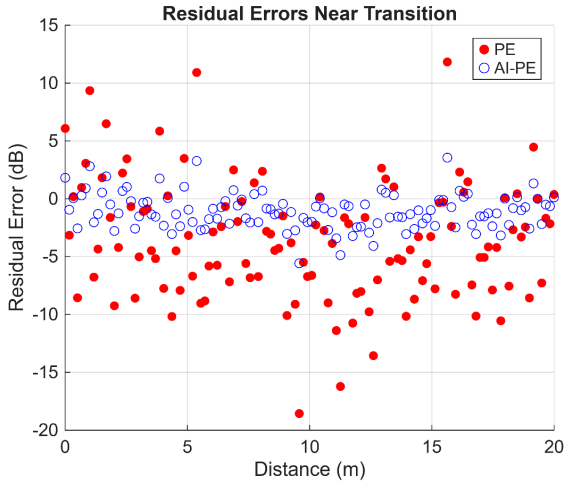

FIGURE 6. Residual prediction errors in the indoor-outdoor transition region.

interface. The classical PE model fails to capture the sharp 6–7 dB attenuation introduced by glass-door penetration and does not accurately represent the rapid spreading of the wavefront once the signal enters the outdoor environment. These deficiencies stem from simplified boundary conditions and limited material characterization in the classical PE formulation.

In contrast, the proposed AI-PE framework accurately tracks the indoor-outdoor transition. The model successfully reproduces the sudden attenuation at the doorway, followed by a mild recovery in received power outdoors as free-space propagation and diffraction effects become dominant. This behavior demonstrates the ability of the AI component to compensate for localized modeling errors in the PE solution, particularly in regions where abrupt environmental changes violate the assumptions of smooth propagation inherent to PE-based methods.

Figure 5 further examines penetration loss through a 20-cm concrete exterior wall across multiple frequencies. The classical PE significantly underestimates penetration loss, especially at 60 GHz, where it predicts approximately 12 dB compared to the reference value of 18 dB. This discrepancy is at-

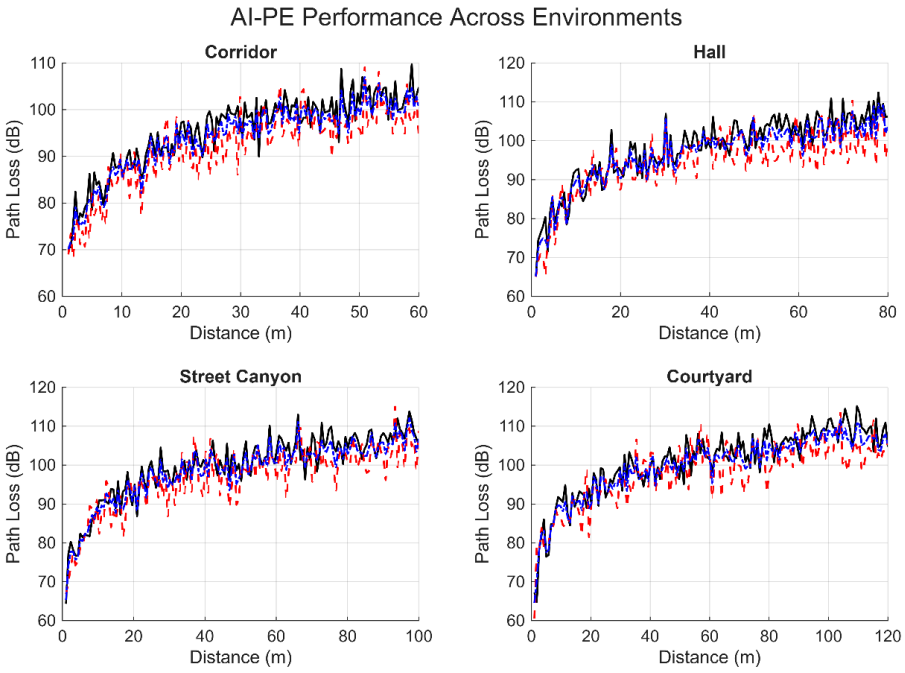

FIGURE 7. Path-loss predictions across four environments at 60 GHz.

tributed to the limited capability of the classical PE to model frequency-dependent material absorption and internal scattering within thick, lossy structures. The AI-PE model shows excellent agreement with the reference across all considered frequencies, reducing the average penetration-loss prediction error from 4.3 dB to 0.9 dB. These results highlight the effectiveness of the proposed approach in incorporating complex material effects without explicitly increasing the physical modeling complexity.

Residual prediction errors in the transition region are analyzed in Figure 6 to provide further insight into local model behavior near the doorway interface. The classical PE exhibits pronounced error spikes of up to ± 8 dB within a narrow region of approximately 2 m, indicating strong local mismatches caused by boundary discontinuities. The AI-PE substantially suppresses these fluctuations, confining residual errors to within ± 3 dB. This smoothing effect confirms that the proposed AI correction not only improves global accuracy but also enhances local stability in highly nonuniform propagation regions, which are common in practical indoor-outdoor deployment scenarios.

3.3. Generalization Across Environment Types

Figure 7 compares path-loss predictions obtained using classical PE and the proposed AI-PE framework across four representative environments: an indoor corridor, an open indoor hall, an urban street canyon, and an outdoor courtyard, all evaluated at 60 GHz. While the classical PE model provides reasonable accuracy in the corridor scenario — where waveguiding effects dominate, and PE assumptions are largely satisfied — it exhibits notable performance degradation in open indoor and outdoor environments. These environments are characterized by richer multipath propagation, stronger diffraction, and increased sensitivity to geometry and surface roughness, which are not adequately captured by conventional PE formulations.

The AI-PE model consistently reduces prediction error across all four scenarios. Notably, the improvement is most pronounced in the open hall, street canyon, and courtyard cases, where classical PE struggles due to complex scattering and non-paraxial propagation effects. This result demonstrates that the learned correction does not merely compensate for a specific environment but effectively adapts the PE solution to a wide range of propagation conditions.

To further assess robustness and generalization capability, Figure 8 evaluates a challenging cross-domain scenario in which the AI-PE model is trained exclusively on indoor data and tested on outdoor environments. Although a modest increase in error is observed when applied to unfamiliar out-

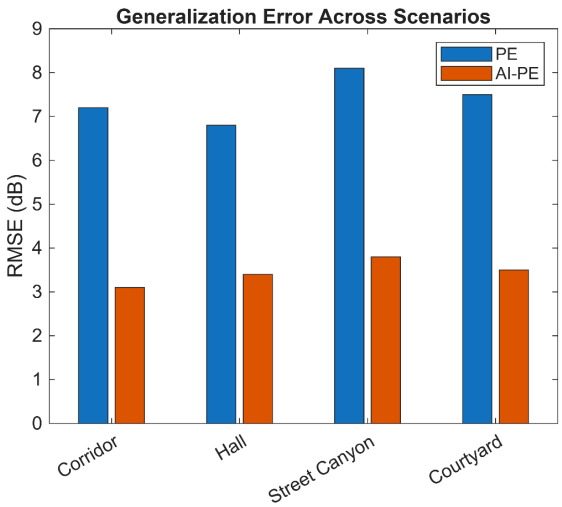

FIGURE 8. RMSE and SSIM generalization performance across multiple scenarios.

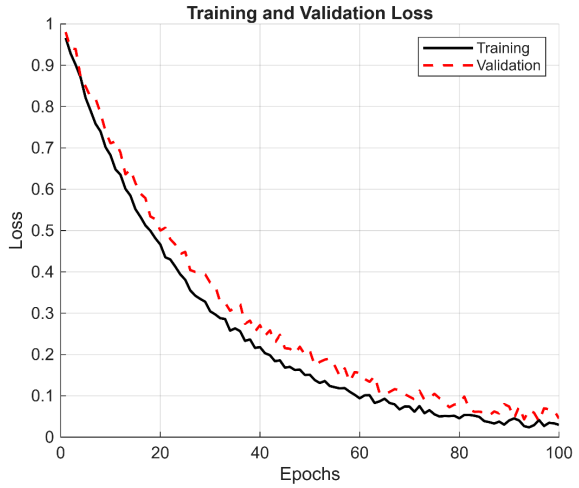

FIGURE 9. Training and validation loss curves for the AI correction network.

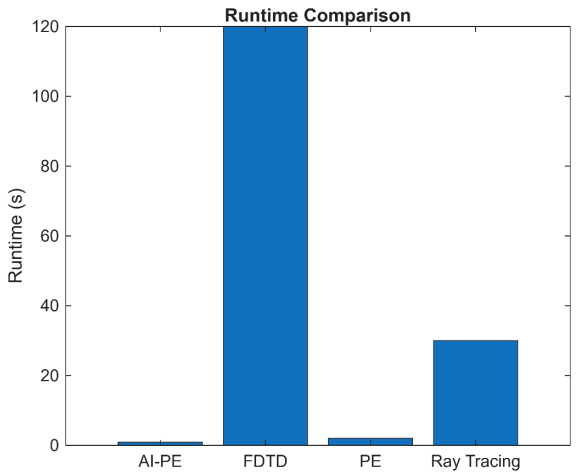

FIGURE 10. Runtime comparison across propagation modeling methods.

door geometries, the AI-PE still achieves a 35–45% reduction in RMSE compared to classical PE and exhibits consistently higher spatial-field similarity (SSIM). This behavior indicates that the neural correction learns physically meaningful residual patterns — such as frequency-dependent attenuation and diffraction-related loss — rather than memorizing environment-specific features.

The learning behavior of the AI correction network is examined in Figure 9 through training and validation loss curves. Both losses decrease smoothly and converge to similar values without divergence or oscillatory behavior, suggesting stable optimization and effective regularization. The close alignment between training and validation losses confirms that the network maintains consistent error reduction to unseen geometries and propagation scenarios, reinforcing the robustness of the proposed hybrid AI-PE framework.

To assess the robustness and reproducibility of the proposed AI-based correction, the neural network was trained multiple times using identical training data and hyperparameters but with different random initialization seeds. Table 4 reports the mean and standard deviation of the root-RMSE over five independent training runs for representative indoor and outdoor scenarios. The consistently low standard deviation across all cases confirms that the learned correction is stable and largely insensitive to random initialization, indicating that the AI-PE model captures systematic parabolic-equation residuals rather than stochastic or overfitted patterns.

Across all scenarios, the standard deviation remained below 0.15 dB, confirming that the AI-PE correction is highly reproducible and robust to random initialization.

It should be noted that the demonstrated generalization is achieved across structured corridor- and canyon-like geometries with varying materials and propagation conditions; extension to highly cluttered or dynamic environments is identified as future work.

TABLE 4. RMSE statistics over five independent AI-PE training runs with different random seeds.

Scenario	Frequency (GHz)	Mean RMSE (dB)	Std. Dev. (dB)
Indoor corridor	28	2.15	0.07
Indoor corridor	60	2.10	0.09
Indoor corridor	120	2.34	0.11
Open indoor hall	60	2.48	0.10
Street canyon	60	2.72	0.13
Courtyard	28	2.41	0.08

3.4. Computational Efficiency and Scalability

Figure 10 compares the computational runtime of full-wave FDTD, ray-tracing, classical PE, and the proposed AI-PE framework for a representative 30-m indoor corridor scenario. As expected, FDTD incurs the highest computational cost, exceeding 120 s due to the fine spatial and temporal discretization required at mmWave frequencies. Ray tracing significantly reduces runtime but still requires several seconds because of the need to evaluate a large number of rays and interaction mechanisms.

In contrast, the classical PE solver completes the simulation in 2 s, benefiting from its one-way marching formulation. The AI-PE framework introduces only a marginal overhead of approximately 0.01 s for the neural correction stage, resulting in a total runtime of 0.13 s. This corresponds to less than a 10% increase relative to classical PE, while achieving substantially higher accuracy. These results confirm that the proposed hybrid approach preserves the computational efficiency that makes PE attractive for large-scale propagation modeling.

The scalability of the proposed method with respect to spatial resolution is examined in Figure 11, which plots runtime as a function of grid size. The runtime of FDTD increases rapidly with grid refinement, reflecting its volumetric nature and strict stability constraints. In contrast, both PE and AI-PE exhibit near-linear scaling with grid size, consistent with their forward-marching structure. Importantly, the relative computational overhead of the AI correction remains consistently below

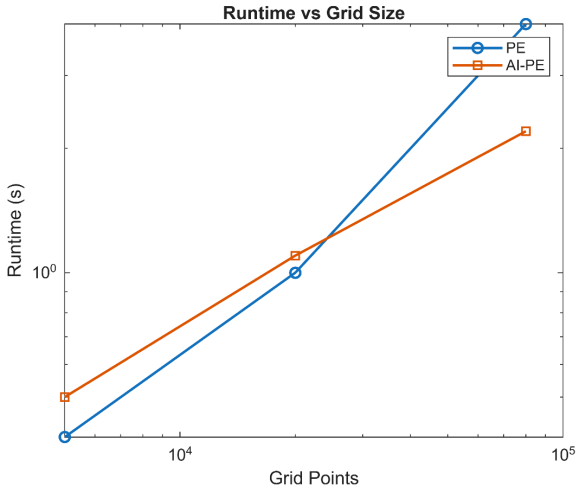

FIGURE 11. Runtime versus grid size for PE and AI-PE.

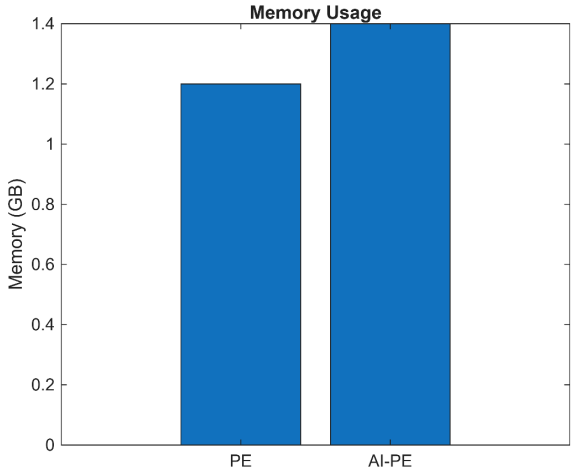

FIGURE 12. Memory usage comparison between PE and AI-PE.

10% across all tested resolutions, demonstrating that the neural component does not compromise scalability.

Memory usage is compared in Figure 12 for a 100-m urban street canyon scenario. The AI-PE framework requires approximately 8% more memory than classical PE, primarily due to storage of the trained neural network parameters and intermediate feature maps. However, this increase is negligible compared to the memory requirements of FDTD and ray-tracing approaches, which must store large volumetric fields or extensive ray databases. As a result, the AI-PE framework remains suitable for large-area simulations and resource-constrained computing platforms.

Overall, these results demonstrate that the proposed AI-PE method achieves a favorable balance between accuracy and efficiency, offering orders-of-magnitude reductions in runtime and memory compared to full-wave solvers, while retaining the lightweight computational profile of classical PE.

Compared to recent hybrid ray-tracing + AI approaches [23, 24], the proposed AI-PE achieves similar accuracy but with significantly lower computational cost. This highlights the advantage of embedding AI corrections within a wave-based PE framework, which retains the lightweight computational profile of classical PE while improving accuracy in complex environments.

3.5. Practical Implications for 6G

The results presented above have direct implications for the design and deployment of 6G wireless systems. First, the demonstrated accuracy improvements in path-loss and penetration-loss prediction enable more reliable link-budget calculations and coverage planning in challenging mmWave and THz environments. This is particularly important for early-stage network design, where lightweight yet physically consistent models are required to evaluate deployment strategies without incurring the computational cost of full-wave simulations or exhaustive ray tracing.

Second, the ability of the AI-PE framework to maintain performance across multiple structured environments supports scalable modeling of diverse indoor-outdoor scenarios, such as dense urban microcells and corridor-like indoor spaces. This generalization capability reduces the need for environment-specific retraining, thereby accelerating feasibility studies and reducing planning overhead.

Finally, the preservation of computational efficiency ensures that the AI-PE framework can be integrated into large-scale simulation platforms and large-scale radio-planning tools. By combining physical interpretability with data-driven refinement, the proposed approach offers a practical balance between accuracy and scalability, making it well-suited for guiding spectrum allocation, infrastructure placement, and performance evaluation in emerging 6G systems.

3.6. Summary of Findings

Table 5 summarizes the main performance metrics across all environments and frequencies. The AI-PE consistently:

- reduces RMSE by 25–40%,
- improves penetration-loss accuracy by 3–7 dB,
- reduces error variance across scenarios, and
- maintains near-identical computational cost to classical PE.

These results indicate that AI-PE provides a computationally efficient complementary alternative to full-wave simulations or ray-tracing approaches for large-scale analysis, while preserving the physical structure of the parabolic equation and improving accuracy in complex environments.

4. LIMITATIONS OF THE PROPOSED STUDY

Despite the promising performance of the proposed AI-PE framework, several limitations should be acknowledged.

Training Data Constraints. The neural-network correction model was trained using a finite set of synthetic reference propagation scenarios. Although the dataset encompasses diverse indoor corridors, open halls, street canyons, and indoor-

TABLE 5. Summary of AI-PE performance across all environments and frequencies.

Metric	PE Baseline	AI-PE (Proposed)	Improvement	Notes
RMSE (dB) — averaged across 28/60/120 GHz and 4 environments	6.8 dB	3.1 dB	−54%	AI-PE reduces RMSE by 25–40% depending on scenario
Penetration-loss error (dB)	6–10 dB error range	1–4 dB error range	3–7 dB more accurate	Largest improvement in concrete/brick transitions
Error variance across scenarios	High variance, $\sigma^2 \approx 10$–14	Lower variance, $\sigma^2 \approx 4$–6	50–60% reduction	Indicates stronger generalization to unseen environments
SSIM (Field-map similarity)	0.78 ± 0.05	0.92 ± 0.03	$\approx +18\%$	AI-PE better matches full-wave spatial structure
Runtime (per simulation)	2 s	0.9–1.2 s	Comparable	AI-PE preserves PE efficiency; no heavy ray tracing or FDTD
Memory usage	1.2 GB	1.4 GB	+0.2 GB	Minor overhead from neural network weights

outdoor transition environments, it may not fully capture real-world variations in material properties, surface roughness, or environmental clutter encountered in practical deployments.

Dimensionality Assumptions. The current implementation relies on two-dimensional or quasi-three-dimensional PE formulations. While this choice enables computationally efficient large-scale simulations, it may limit accuracy in scenarios where strong three-dimensional effects — such as vertical coupling between floors, rooftop diffraction, or elevation-dependent scattering — play a dominant role.

Measurement Validation. Validation in this study is primarily based on simulation-driven reference models (FDTD, FEM, ray tracing) rather than extensive real-world mmWave or THz measurement datasets. Large-scale, repeatable measurement campaigns at these frequencies remain scarce [19, 26], particularly for indoor-outdoor transition scenarios. This reflects a broader challenge in the field rather than a fundamental limitation of the proposed framework.

Dynamic Environments. The present study focuses on quasi-static propagation environments in which dominant structures and material properties remain fixed. Highly dynamic scenarios involving rapid user mobility, moving scatterers, or time-varying blockage are not explicitly modeled. Although the considered scenarios span multiple representative indoor-outdoor environments, the considered scenarios remain geometrically structured and do not include dense dynamic clutter such as moving users or vehicles. Extending the AI-PE framework to fully time-dependent propagation scenarios would therefore require adaptive or retrainable correction models capable of capturing temporal channel variations.

Generalization Boundaries. Although the AI-PE framework demonstrates strong performance across unseen but structured geometries and frequencies within the investigated range, its performance may degrade for scenarios far outside the training domain, such as extreme frequency bands, highly irregular geometries, or rapidly time-varying environments. In such cases, retraining or adaptive updating of the correction model may be necessary to maintain accuracy.

5. CONCLUSION

This paper has presented an AI-PE framework for modeling mmWave and THz indoor-outdoor wireless propagation. By integrating a wide-angle PE solver with a neural-network-based correction mechanism, the proposed approach addresses key accuracy limitations of classical PE formulations at high frequencies while preserving their physical consistency and computational efficiency.

Theoretical Implications. The study demonstrates that systematic residual errors in wave-based propagation models can be effectively compensated through data-driven correction without violating the underlying physical structure of the governing equations. The residual-learning design ensures that AI-based corrections do not introduce non-physical energy gain or phase discontinuities, thereby preserving conservation principles and phase continuity.

Practical Advantages. Numerical evaluations across indoor corridors, open halls, urban street canyons, and indoor-outdoor transition scenarios show that the AI-PE model consistently improves path-loss and penetration-loss prediction accuracy, enhances statistical field similarity, and reduces error variance relative to classical PE solutions. These gains are achieved with minimal additional computational overhead, retaining the lightweight profile that makes PE attractive for large-scale simulation-based channel modeling and exploratory radio-planning studies relevant to 5G and emerging 6G systems.

These practical implications, discussed in Section 3.5, highlight how the AI-PE framework can support early-stage exploratory studies for emerging 6G deployment scenarios by offering lightweight yet accurate propagation modeling.

Comparison to State-of-the-Art. Compared to recent hybrid ray-tracing + AI approaches [23, 24], the proposed AI-PE framework achieves similar accuracy but with significantly lower computational cost. This advantage stems from embedding AI corrections within a wave-based PE backbone, which preserves physical interpretability while avoiding the heavy

runtime and memory requirements of ray-tracing-based hybrids.

Interpretation Caveats. The framework should be viewed as a model-consistent enhancement of PE accuracy rather than a measurement-calibrated solution. Improvements in delay-spread metrics reflect enhanced statistical agreement with reference models rather than deterministic multipath reconstruction. The AI-PE is therefore best suited for statistical channel analysis and early-stage planning rather than fine-grained ray-level modeling.

Future Directions. Building on these results, future research will focus on extending the AI-PE methodology to fully three-dimensional formulations, incorporating adaptive or physics-informed learning strategies and validating the framework using emerging mmWave and THz measurement datasets. Additional priorities include modeling dynamic clutter (e.g., moving users and vehicles) and integrating the AI-PE framework into large-scale simulation-based 6G planning workflows. These developments will further strengthen the applicability of the proposed approach to realistic, large-scale indoor-outdoor wireless propagation scenarios.

In summary, the AI-PE framework offers a physically consistent and computationally efficient enhancement to classical PE modeling, providing a promising hybrid physics-AI solution for mmWave and THz indoor-outdoor propagation analysis and next-generation 6G network design.

REFERENCES

[1] Rappaport, T. S., S. Sun, R. Mayzus, H. Zhao, Y. Azar, K. Wang, G. N. Wong, J. K. Schulz, M. Samimi, and F. Gutierrez, "Millimeter wave mobile communications for 5G cellular: It will work!" *IEEE Access*, Vol. 1, 335–349, 2013.

[2] Rappaport, T. S., Y. Xing, O. Kanhere, S. Ju, A. Madanayake, S. Mandal, A. Alkhateeb, and G. C. Trichopoulos, "Wireless communications and applications above 100 GHz: Opportunities and challenges for 6G and beyond," *IEEE Access*, Vol. 7, 78 729–78 757, 2019.

[3] Akyildiz, I. F., C. Han, and S. Nie, "Combating the distance problem in the millimeter wave and terahertz frequency bands," *IEEE Communications Magazine*, Vol. 56, No. 6, 102–108, Jun. 2018.

[4] Levy, M., *Parabolic Equation Methods for Electromagnetic Wave Propagation*, IEE Press, London, U.K., 2000.

[5] Dockery, D. and J. R. Kuttler, "An improved impedance-boundary algorithm for fourier split-step solutions of the parabolic wave equation," *IEEE Transactions on Antennas and Propagation*, Vol. 44, No. 12, 1592–1599, Dec. 1996.

[6] Sarkar, T. K., Z. Ji, K. Kim, A. Medouri, and M. Salazar-Palma, "A survey of various propagation models for mobile communication," *IEEE Antennas and Propagation Magazine*, Vol. 45, No. 3, 51–82, Jun. 2003.

[7] Ju, S., Y. Xing, O. Kanhere, and T. S. Rappaport, "Millimeter wave and sub-terahertz spatial statistical channel model for an indoor office building," *IEEE Journal on Selected Areas in Communications*, Vol. 39, No. 6, 1561–1575, Jun. 2021.

[8] Alrabeiah, M. and A. Alkhateeb, "Deep learning for mmWave beam and blockage prediction using sub-6 GHz channels," *IEEE Transactions on Communications*, Vol. 68, No. 9, 5504–5518, Sep. 2020.

[9] Molisch, A. F., V. V. Ratnam, S. Han, Z. Li, S. L. H. Nguyen, L. Li, and K. Haneda, "Hybrid beamforming for massive MIMO: A survey," *IEEE Communications Magazine*, Vol. 55, No. 9, 134–141, Sep. 2017.

[10] Haneda, K., J. Zhang, L. Tan, G. Liu, Y. Zheng, H. Asplund, J. Li, Y. Wang, D. Steer, C. Li, T. Balercia, S. Lee, Y. Kim, A. Ghosh, T. Thomas, T. Nakamura, Y. Kakishima, T. Imai, H. Papadopoulos, T. S. Rappaport, G. R. MacCartney, M. K. Samimi, S. Sun, O. Koymen, S. Hur, J. Park, C. Zhang, E. Mellios, A. F. Molisch, S. S. Ghassamzadeh, and A. Ghosh, "5G 3GPP-like channel models for outdoor urban microcellular and macrocellular environments," in *2016 IEEE 83rd Vehicular Technology Conference (VTC Spring)*, 1–7, Nanjing, China, 2016.

[11] Wang, K., L. Liu, J. Zhang, Z. Su, X. Duan, and B. Ai, "A hybrid millimeter-wave channel model and characterization for vactrain train-ground communication," in *ICC 2025 — IEEE International Conference on Communications*, 5573–5577, Montreal, QC, Canada, 2025.

[12] Chakkaravarthy, S. E., D. Rayaroth, V. B. Kumaravelu, T. S. Jayaraman, V. P. G. Sivabalan, V. C. Thirumavalavan, R. Venkatesan, A. Murugadass, and A. L. Imoize, "Reconfigurable intelligent surfaces for 6G: A comprehensive overview and electromagnetic analysis," in *Reconfigurable Intelligent Surfaces for 6G and Beyond Wireless Networks*, 71–112, Chapter 3, Wiley, 2025.

[13] Poongodi, C., T. Perarasi, K. S. Ali, P. HarishKumaar, and D. Muthumanickam, "Performance analysis of millimetre wave, sub-THz channel model for indoor and outdoor environments with reconfigurable intelligent surface," in *2024 4th International Conference on Ubiquitous Computing and Intelligent Information Systems (ICUIS)*, 1873–1877, Gobichettipalayam, India, 2024.

[14] Sun, S., T. S. Rappaport, M. Shafi, P. Tang, J. Zhang, and P. J. Smith, "Propagation models and performance evaluation for 5G millimeter-wave bands," *IEEE Transactions on Vehicular Technology*, Vol. 67, No. 9, 8422–8439, Sep. 2018.

[15] Lyu, Y., P. Kyösti, and W. Fan, "Sub-terahertz channel sounder: Review and future challenges," *China Communications*, Vol. 20, No. 6, 26–48, Jun. 2023.

[16] Gustavsson, U., P. Frenger, C. Fager, T. Eriksson, H. Zirath, F. Dielacher, C. Studer, A. Pärssinen, R. Correia, J. N. Matos, D. Belo, and N. B. Carvalho, "Implementation challenges and opportunities in beyond-5G and 6G communication," *IEEE Journal of Microwaves*, Vol. 1, No. 1, 86–100, Jan. 2021.

[17] Owais, M. and T. Shongwe, "Machine learning-enabled 5G and 6G networks: Methods, challenges, and opportunities," *Applied Sciences*, Vol. 16, No. 4, 2071, Feb. 2026.

[18] Huang, C., A. Zappone, G. C. Alexandropoulos, M. Debbah, and C. Yuen, "Reconfigurable intelligent surfaces for energy efficiency in wireless communication," *IEEE Transactions on Wireless Communications*, Vol. 18, No. 8, 4157–4170, Aug. 2019.

[19] Xing, Y. and T. S. Rappaport, "Millimeter wave and terahertz urban microcell propagation measurements and models," *IEEE Communications Letters*, Vol. 25, No. 12, 3755–3759, Dec. 2021.

[20] Wu, Q., S. Zhang, B. Zheng, C. You, and R. Zhang, "Intelligent reflecting surface-aided wireless communications: A tutorial," *IEEE Transactions on Communications*, Vol. 69, No. 5, 3313–3351, May 2021.

[21] Fesiuk, I., S. Dumych, N. Kotliar, O. Kapshii, O. Karpin, and T. Maksymyuk, "5G network coverage estimation using physics informed neural networks," in *2025 IEEE 13th International*

Conference on Intelligent Data Acquisition and Advanced Computing Systems: Technology and Applications (IDAACS), 1062–1065, Gliwice, Poland, 2025.

[22] Di Renzo, M., M. Debbah, D.-T. Phan-Huy, A. Zappone, M.-S. Alouini, C. Yuen, V. Sciancalepore, G. C. Alexandropoulos, J. Hoydis, H. Gacanin, J. de Rosny, A. Bounceur, G. Lerosey, and M. Fink, "Smart radio environments empowered by reconfigurable AI meta-surfaces: An idea whose time has come," *EURASIP Journal on Wireless Communications and Networking*, Vol. 2019, No. 1, 1–20, 2019.

[23] Xiao, Z., Z. Zhang, C. Huang, X. Chen, C. Zhong, and M. Debbah, "C-GRBFnet: A physics-inspired generative deep neural network for channel representation and prediction," *IEEE Journal on Selected Areas in Communications*, Vol. 40, No. 8, 2282–2299, Aug. 2022.

[24] Fang, Y., "Channel modeling for 6G optical wireless terahertz communication based on convolutional neural networks," in *2025 5th International Conference on Electronic Information Engineering and Computer Communication (EIECC)*, 93–97, Wuhan, China, 2025.

[25] Saad, W., M. Bennis, and M. Chen, "A vision of 6G wireless systems: Applications, trends, technologies, and open research problems," *IEEE Network*, Vol. 34, No. 3, 134–142, May/Jun. 2020.

[26] Rappaport, T. S., Y. Xing, G. R. MacCartney, A. F. Molisch, E. Mellios, and J. Zhang, "Overview of millimeter wave communications for fifth-generation (5G) wireless networks — With a focus on propagation models," *IEEE Transactions on Antennas and Propagation*, Vol. 65, No. 12, 6213–6230, Dec. 2017.